Discrimination between rough and smooth interfaces of multilayers inside a multilayer stack using high-energy electron scattering

1996 J. Phys.: Condens. Matter 8 649

(http://iopscience.iop.org/0953-8984/8/6/006)

J. Phys.: Condens. Matter **8** (1996) 649–663. Printed in the UK

Discrimination between rough and smooth interfaces of multilayers inside a multilayer stack using high-energy electron scattering

J Zweck, M Tewes† and H Hoffmann

Institut für Angewandte Physik der Universität Regensburg, D-93040 Regensburg, Germany

Received 25 September 1995, in final form 9 November 1995

Abstract. The interface quality of multilayer thin-film systems is of great interest for both the understanding of the physical properties which result from the loss of symmetry at the interfaces and for application purposes. We describe a technique which uses high-energy electron radiation (300 keV) from a conventional transmission electron microscope to characterize in a scattering experiment the interface quality of such multilayer systems. The technique is based on the use of high-energy electrons, with a correspondingly large k-vector $\boldsymbol{k}$, which leads to a Ewald sphere with radius $|\boldsymbol{k}|$. This Ewald sphere can for many practical purposes be approximated by a plane. Therefore, the information obtained in a scattering experiment is restricted to a plane perpendicular to the primary beam, i.e. parallel to the multilayer structure, when the electrons pass through the multilayer system along its normal vector. When pair distribution functions (pdfs) are calculated from the scattered intensities, information can be gained about the coordination of pairs of atoms of different kinds within a plane *parallel* to the multilayer structure only. This information can then be used to determine whether the atoms at the interfaces between layers of different types of atom *inside* the multilayer stack are intermixed or not intermixed on an atomic scale. The technique is described, and its use is demonstrated on an $[Fe/Tb]_N$ multilayer system which has been prepared in order to create both sharp interfaces and interfaces which are intermixed. A comparison with an amorphous alloy of the same nominal composition is also given.

1. Introduction

Multilayer thin films are now widely used in modern technology due to their physical properties which differ significantly from those of non-multilayered materials [1, 2]. One possible reason for this difference can be the lack of symmetry at the interfaces between the individual layers of different materials. From the above it is immediately obvious that from a multilayer specimen with a perfectly sharp (i.e. non-intermixed) interface, physical properties can be expected that are different to those for a specimen with a diffusion zone at the interface [3, 4]. In the latter case, a gradual change of composition from one layer to the other occurs. In this case the alloyed region at the interface will not show the same properties as are to be expected when the interfaces in a multilayer stack are perfect (i.e. non-intermixed). For detailed studies of the influence of the interfaces on the physical properties of these materials it is necessary to know whether the interfaces which are under consideration are sharp or rough, or preferably the degree of intermixing of atoms from adjacent layers at the interface.

† Now at: SAP Company, Heidelberg, Germany.

0953-8984/96/060649+15$19.50

In this paper we describe a method for determining the roughness of interface layers using electron diffraction, followed by a subsequent calculation of pair distribution functions. There are two main differences between the method being proposed and the other commonly used methods such as SAXS and specular x-ray reflectometry. Firstly, due to the use of high-energy electrons (300 keV) a planar sensing of the multilayer structure can be achieved. Secondly, no fitting of experimental intensity data with numerous parameters, which are usually difficult to control with respect to their physical meaningfulness, is required. Instead, a rather straightforward calculation of planar pair distribution functions yields the results directly. In the following, we describe the basic technique and its advantages. We apply the technique to two differently prepared multilayer systems, which differ mainly in their interface roughnesses.

2. Theoretical considerations

The method is based on the scattering of high-energy electrons of 300 keV in a commercially available electron microscope (Philips CM30) with remote control facility. The main point in the use of high-energy electrons is the huge k-vector of these compared to the usual k-vectors in x-ray experiments for structure investigations. The obtainable k-vector for 300 keV electrons ($\lambda_{\mathrm{el}}^{300\ \mathrm{keV}} = 1.97$ pm) yields approximately 3000 nm^{-1}, whereas for Mo Kα radiation ($\lambda_{\mathrm{K}\alpha}^{\mathrm{Mo}} = 0.154$ nm) the obtainable length of the k-vector for the incoming radiation is only 87 nm^{-1}. Thus, in reciprocal space, the Ewald sphere for high-energy electrons will have a radius of approximately 35 times the radius of that for x-ray radiation. The consequences of this large radius of the Ewald sphere are fairly obvious: when a scattering experiment is performed, the Ewald sphere can be considered for many practical purposes to be a 'Ewald plane' and this will have a useful impact on the experiments as described below. The experiments consist in the performance of electron scattering experiments with a subsequent calculation of **p**lanar **p**air **d**istribution **f**unctions ($\mathrm{p}^2\mathrm{dfs}$), which can then be interpreted in terms of an intermixed or non-intermixed interface layer. To understand the information contained in the $\mathrm{p}^2\mathrm{dfs}$, a description of the physics involved will be given.

A very important point is the way in which the scattering experiment gives information about a specimen under investigation. As is well known, the scattering experiment can be described as a sensing of the three-dimensional Fourier transform of the structure under investigation by the Ewald sphere [5, 6]. For single-crystalline specimens, the non-zero scattered intensity is—due to their perfectly periodic lattices—confined to the reciprocal-lattice spots only.

So far, no contribution to the diffracted intensity, stemming from grain boundaries or lattice imperfections, has been taken into account. These contributions are non-periodic, and therefore do not yield information in reciprocal space which is confined to certain locations. In contrast, the contribution of the non-periodic features appears between and around the reciprocal-lattice spots, because the Fourier transform of non-periodic features gives a broad distribution of spatial frequencies in reciprocal space. The same is true for interfaces, where a transition between different materials with (in general) different structures occurs. Although a multilayer structure is periodic on a nanometre scale, it does cause a disruption of the symmetry on an atomic scale close to the interface, and therefore contributes to the diffuse scattering. Finally, the modification of the three-dimensional Fourier spectrum of a multilayered specimen, where each individual layer is either polycrystalline or even amorphous, appears fairly complicated.

To get an impression of the modulus of a three-dimensional Fourier spectrum (the

so-called power spectrum) an ideal multilayer specimen, i.e. with no intermixing at the interfaces, will be considered in the following. Then, the sequence of layers A and B can formally be described by the sum for layers A only plus that for layers B only. This is shown schematically in figure 1 for a specimen where each individual layer is made up of perfectly ordered atoms with a specific interatomic distance. In figure 1(a), the initial infinite periodic lattice sites of the two different lattices (denoted 'type A' and 'type B'), represented by delta functions, are given. In figure 1(b), the layer functions $L_{A/B}(z)$ are given, which are needed in this formal description to form the substructures of the multilayer system. These layer functions are given by

$$L_A(z) = \begin{cases} 1 & \text{if atoms of type 'A' are present in depth } z \text{ of the multilayer system} \\ 0 & \text{if no atoms of type 'A' are present in depth } z \end{cases} \tag{1}$$

and

$$L_B(z) = \begin{cases} 1 & \text{if atoms of type 'B' are present in depth } z \text{ of the multilayer system} \\ 0 & \text{if no atoms of type 'B' are present in depth } z. \end{cases} \tag{2}$$

Additionally, in order to fill the whole space,

$$L_A(z) + L_B(z) = 1 \tag{3}$$

for all values of z. A multiplication of the atomic position functions in figure 1(a) and the layer functions in figure 1(b) yields the sublattices of the different types of atom as shown in figure 1(c). These can then be combined by simple addition to the complete, yet still infinitely periodic multilayer structure given in figure 1(d). In order to get the function which represents the multilayer system of finite thickness, another multiplication by a layer thickness function $T(z)$ is needed (see figure 1(e)), which finally yields the multilayer system. This system consists in our example of only two layers of atoms of type 'B' (with 10 'atoms' each) and one centre layer of atoms of type 'A' (8 'atoms'), as shown in figure 1(f).

The Fourier transform of this multilayer structure can then be seen to be the sum of the Fourier transforms of the individual layer structures (figure 2).

The initially infinite periodic arrangements of atoms in real space lead to the reciprocal-lattice points indicated in figure 2(a). The modulus of the Fourier transform of the layer function is given in figure 2(b), which is convoluted with the reciprocal-lattice points, denoted by the symbol $\otimes$ between figures 2(a) and 2(b). Therefore, all reciprocal-lattice points that correspond to layer A will be convoluted with the corresponding function FT$\{L_A(z)\}$, where the symbol FT{ } stands for the Fourier transform operation. Correspondingly, the reciprocal-lattice points of layer B will be convoluted by FT$\{L_B(z)\}$. In total, the Fourier spectrum of the crystalline lattice will be modified by the convolution in a way that gives subsidiary components to all reciprocal-lattice points, which contain the information on the multilayer periodicity. The resulting reciprocal lattices of type 'A' and 'B' (figure 2(c)) are then summed to yield the total Fourier spectrum of the infinitely periodic multilayer (figure 2(d)). To take into account the influence of the Fourier transform of the layer thickness function FT$\{T(z)\}$ (figure 2(e)), again a convolution operation has to be performed, which finally yields the Fourier components of the multilayer sequence of figure 1(f). Since this is a complex function, only the modulus (the power spectrum) is given here.

If a multilayer structure is assumed, which is single crystalline within each individual layer and extends laterally (i.e. within the x–y-plane, perpendicular to the electron beam) to infinity, then it is clear from the above that in reciprocal space one will find laterally (i.e. in

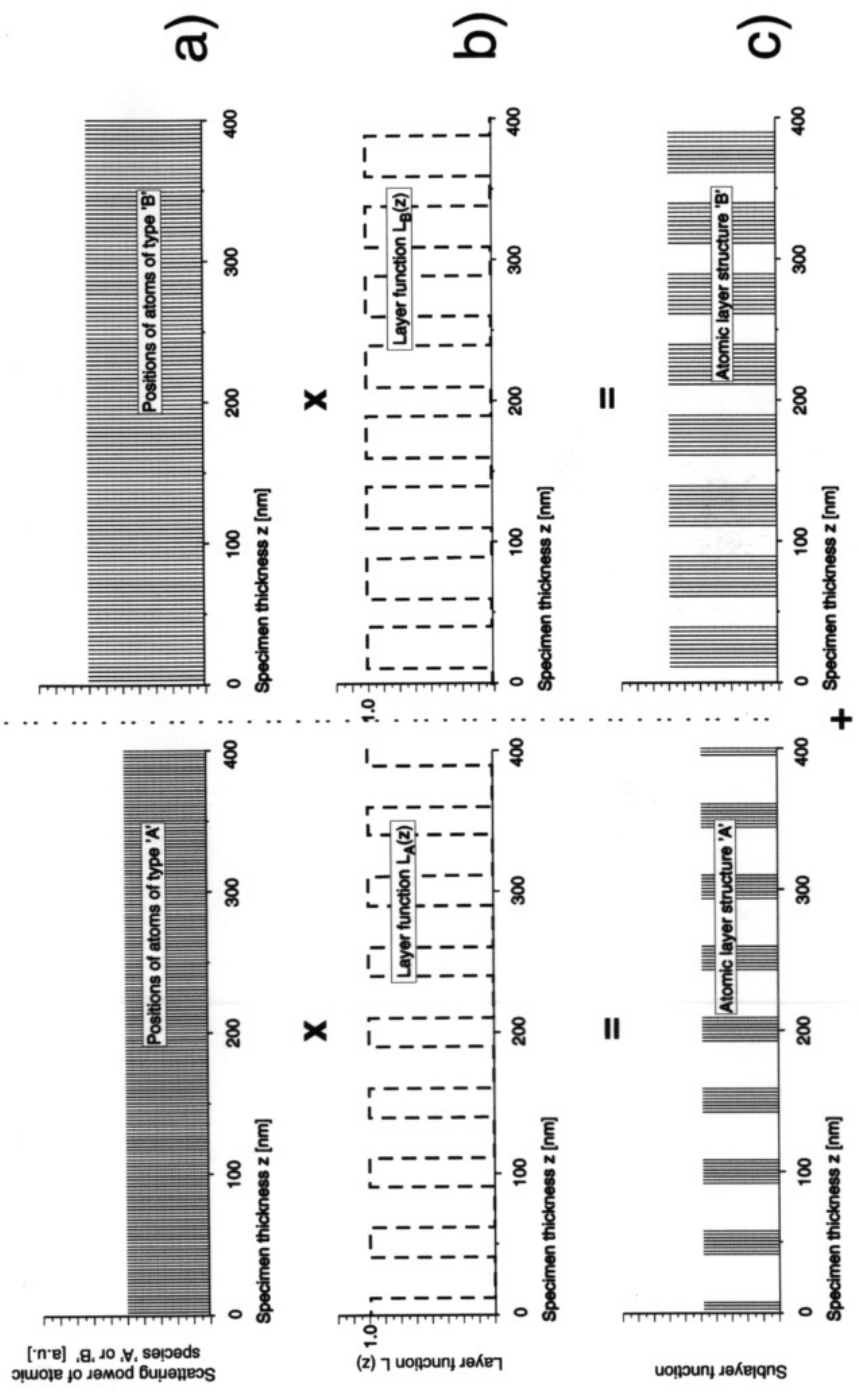
a)
b)
c)
Positions of atoms of type 'B'
Positions of atoms of type 'A'
Layer function $L_B(z)$
Layer function $L_A(z)$
Atomic layer structure 'B'
Atomic layer structure 'A'
Specimen thickness z [nm]
Scattering power of atomic species 'A' or 'B' [a.u.]
Layer function L (z)
Sublayer function
1.0
0
100
200
300
400
x
=
+

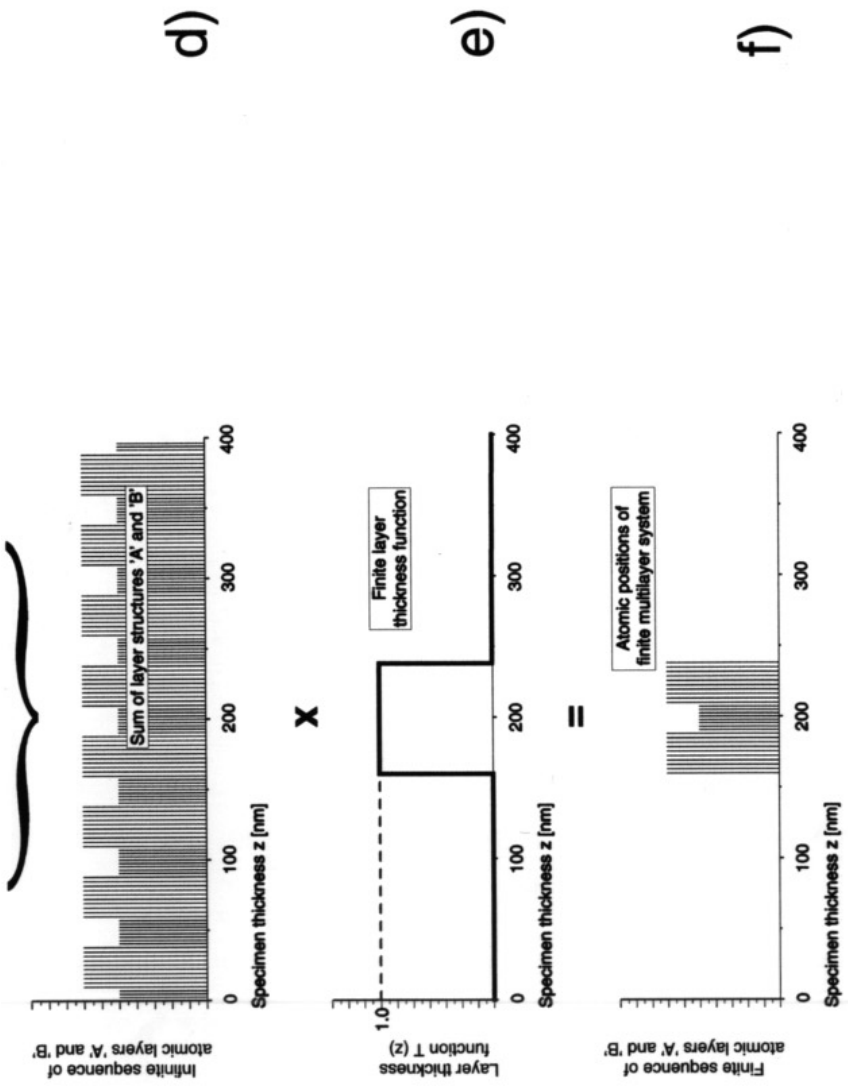

Figure 1. A schematic representation of the formal description of a multilayer stack in real space. The multilayer stack is composed of the sum of two infinite arrays of different atoms (represented by delta functions of different spacings and amplitudes, (a)), multiplied by a layer function $L_{A/B}(z)$, (b), and truncated to a finite thickness of the total stack, (f), by a layer thickness function $T(z)$, (e).

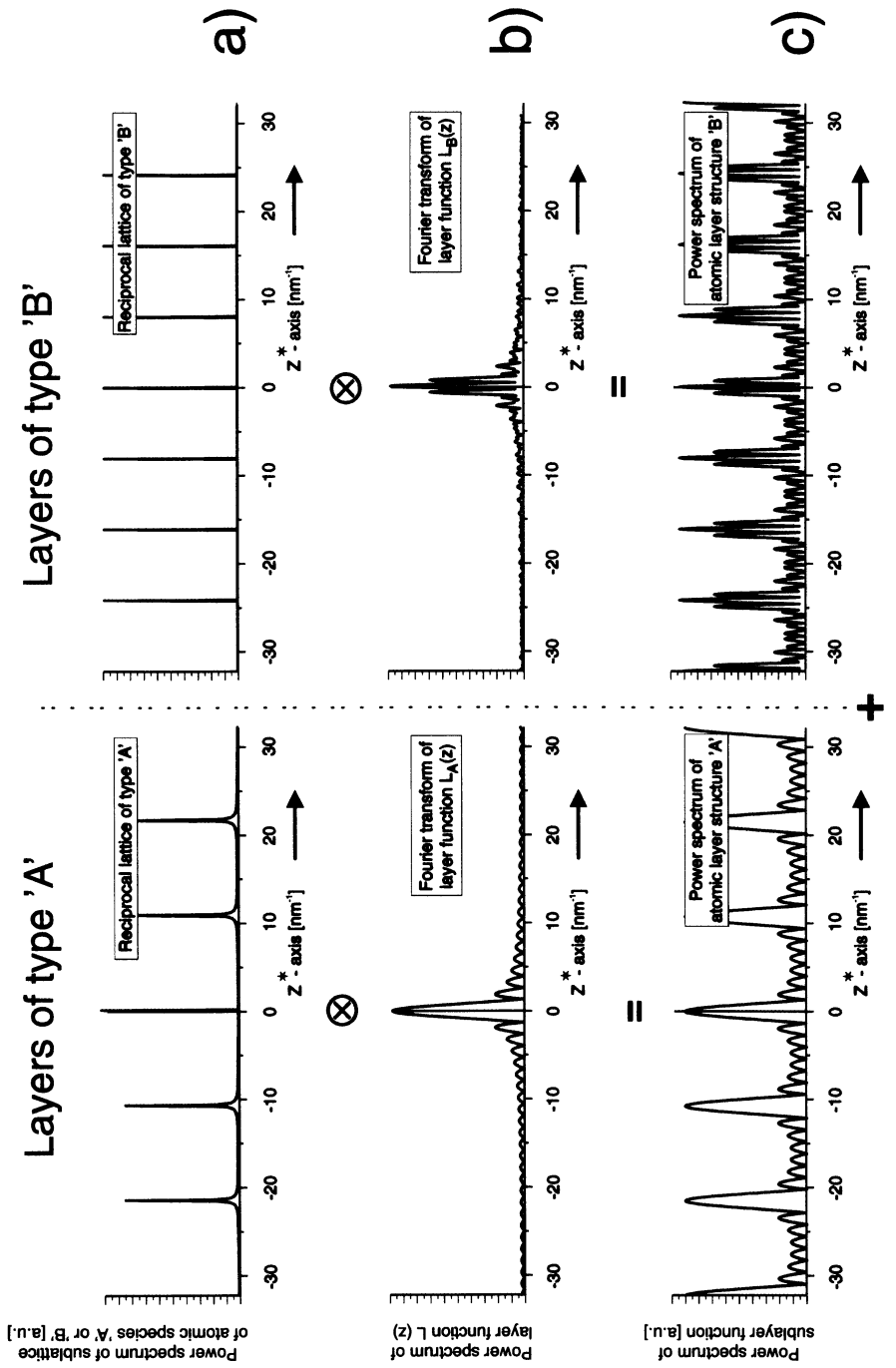
Layers of type 'A'
Layers of type 'B'
a)
b)
c)
Reciprocal lattice of type 'A'
Reciprocal lattice of type 'B'
Fourier transform of layer function $L_A(z)$
Fourier transform of layer function $L_B(z)$
Power spectrum of atomic layer structure 'A'
Power spectrum of atomic layer structure 'B'
z* - axis [nm^{-1}]
-30
-20
-10
0
10
20
30
Power spectrum of sublattice of atomic species 'A' or 'B' [a.u.]
Power spectrum of layer function L (z)
Power spectrum of sublayer function [a.u.]

Figure 2. A schematic representation of the formal description of a multilayer stack in reciprocal space. The multilayer stack is composed of the sum of the Fourier transforms of two infinite arrays of atoms (represented by the reciprocal-lattice points as delta functions of different spacings and amplitudes, (a), convoluted with the Fourier transform of a truncated layer structure function $\mathrm{FT}\{L_{A/B}(z) \times T(z)\}$, (b) and (c). Note, that in reciprocal space the arithmetic operation $\times$ used in real space (figure 1) becomes $\otimes$. The result (f) still shows the reciprocal-lattice points of the different layer structures, but broadened due to the convolution and superimposed in k-space.

the x^*-y^*-plane of the reciprocal lattice) reciprocal-lattice points just as in the case of an ideal single crystal which can be thought to consist of a large elementary cell (a so-called 'super-cell'). This super-cell describes the stacking of layers of different thicknesses and of different species of atom. In the direction perpendicular to the x^*–y^*-plane, the reciprocal-lattice points are no longer strictly 'points', but are broadened due to the convolution with the Fourier transform of the specimen's layer function FT$\{L_{A/B}(z)\}$ and layer thicknesses function FT$\{T(z)\}$. This is a very well-known fact in the area of electron diffraction of thin crystals.

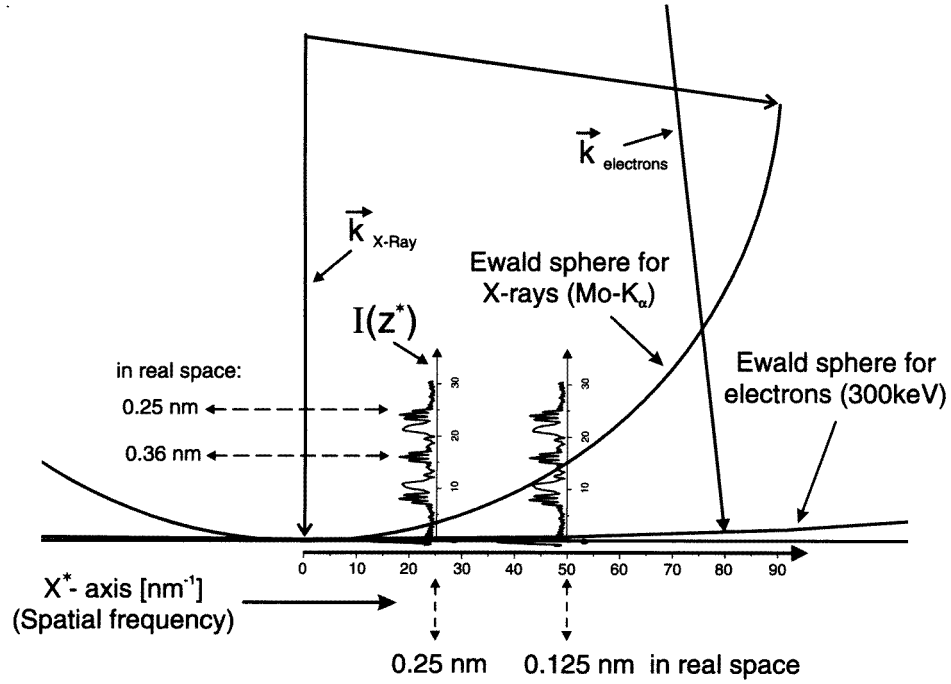

Figure 3. A schematic representation of the deviation of the Ewald sphere from the x^*–y^*-plane for x-ray radiation and high-energy electrons (300 keV). The x^*–y^*-plane is represented by the x^*-axis only. For x-rays, practically no planar sensing of the x^*–y^*-plane is possible, whereas for high-energy electrons, the Ewald sphere can be described by a plane for a large range of spatial frequencies. Due to the deviation of the Ewald sphere from the x^*–y^*-plane for x-rays, the reciprocal-lattice points, which are broadened due to the external shape of the thin film, are intersected at points of different intensities. However, for high-energy electrons the situation is much more favourable.

But while for thin layers of one species only, the typical shape of the broadening function is fairly simple (namely, the Fourier transform of a step function that describes the thickness of the thin layer), the corresponding function for a multilayer system is much more complicated. This imposes fairly strict limitations on the scattering measurements that can be performed on these multilayer systems: since the measurable intensity is given by the square modulus of the Fourier transform of both the atomic arrangement within and the overall shape of the specimen, the modulation in the z^*-direction (i.e. along the direction of the incoming beam) also has to be taken into account. This means that it is not sufficient to measure only a radial trace of scattered intensity starting from the central beam spot. With increasing distance from the central beam the Ewald sphere will deviate successively

further from the x^*–y^*-plane, and not only the intensity variations within the x^*–y^*-plane, but also to a certain extent the variation in z^*-direction will be registered. This situation is shown schematically in figure 3 for the thin multilayer specimen of figure 1: due to the broadening of the reciprocal-lattice points with subsidiary maxima, the intersection of the Ewald sphere (drawn for x-ray radiation) with the reciprocal-lattice points will give different intensities depending on the distance x^* from the k-space origin due to its deviation from the x^*–y^*-plane.

The advantage of the use of high-energy electrons becomes obvious. In figure 3, the same situation as given in the case of x-rays is shown for 300 keV electrons as the radiation source. Due to the larger value of the primary k-vector by a factor of approximately 35, the Ewald sphere is essentially flat over a much larger range of spatial frequencies in reciprocal space, and therefore to a good approximation allows the registration of scattered intensity in the x^*–y^*-plane only. These intensity data can then be used to calculate the p^2df for a multilayered specimen that yields information from the distribution of atoms in the x–y-plane only.

If the interfaces between layers of atoms 'A' and 'B' are perfectly sharp, no pairs of different atomic species from layer A and from layer B should be observed. Only pairs of atoms of the same type, like A–A or B–B, can be seen. On the other hand, if there is some intermixing present, A–B pairs should also be detectable, because then the orientation of their connecting axis will not only be perpendicular to the x–y-plane but also lie to a certain extent in the x–y-plane. This, in turn, gives rise to maxima in the p^2df which correspond to the interatomic distances of the different pairs of atoms. A schematic representation of this situation is given in figure 4.

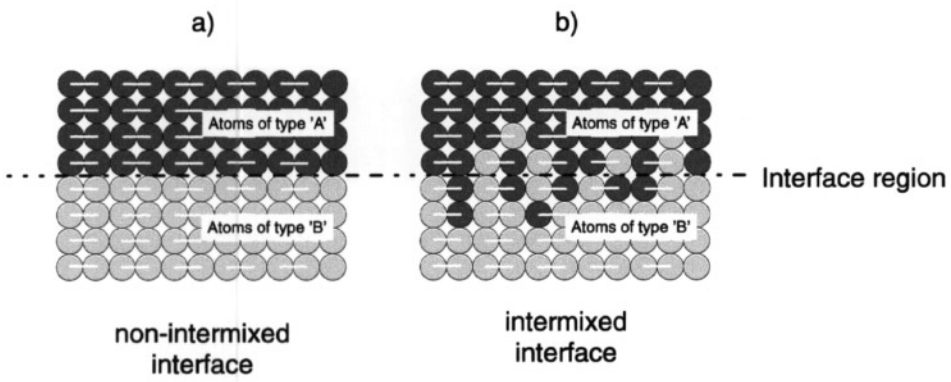

Figure 4. A schematic representation of the arrangement of pairs of atoms (A–A, A–B, B–B) for (a) a perfect non-intermixed interface and (b) an intermixed interface. The in-plane coordination is indicated by white lines connecting the neighbouring atoms. In (a) no pairs of type A–B are present, whereas in (b) A–B pairs will be observable.

In the following, an experiment is described showing the difference between the p^2dfs of multilayered thin films which have been intentionally prepared in such a way as to either minimize the degree of intermixing at the interfaces or to allow a certain degree of intermixing. The specimens have been investigated by high-energy electron diffraction (HEED), and from the intensity measurements their corresponding p^2dfs have been calculated.

3. Specimens

The specimens used for the investigations were sputtered multilayered thin films consisting of layers of Fe and Tb. Each of the multilayer films was 100 nm thick, and was formed by alternating layers of Fe and Tb. The preparation was different for the two kinds of specimen. One specimen was prepared using shutters for targets both of Fe and Tb, and the deposition process was performed by alternately opening the shutters for a certain time which resulted in layers of thickness 1.2 nm for both Fe and Tb. This multilayer film is assumed to have rather sharp interfaces (figure 4(a)) of Fe and Tb, and will be referred to in the following as 'the sharp-interface film'. 'The intermixed-interface film' was then realized with the plasma of both targets in the sputter deposition equipment ignited, while also both of the shutters were opened. The layer structure was then deposited by rotating the substrate successively over both of the targets, which yielded layer thicknesses of 1.2 nm of Fe and 1.8 nm of Tb. Additionally, since the plasma volumes above the two targets did overlap to a certain degree, between the targets there was a mixture of Fe and Tb atoms with their concentrations depending on the distance of the substrate from the targets. Therefore, no sharp interfaces can be expected from this type of specimen preparation. Instead, a compositionally modulated layer structure is to be expected, with a high degree of intermixing of unlike atoms in the interface regions (figure 4(b)). The assumption of a sharp interface in the case of the first preparation procedure described above is based both on the method of preparation, which should create sharp interfaces, as well as on the measurements of magnetic properties. From these, a clear difference can be observed between the magnetic anisotropies perpendicular to the multilayer film plane of the differently prepared multilayer specimens. This difference can easily be explained, when it is related to sharp or intermixed interfaces, correspondingly [14].

The individual layers were amorphous, as has been found from the diffraction patterns. (It should be noted here that the diffraction pattern showed crystalline reflections when the layer thicknesses were 1.8 nm of Fe and 1.2 nm of Tb. The crystalline contributions to the diffraction pattern were from Fe, which obviously crystallizes when a certain thickness of approximately 1.8–2.0 nm is reached. Additionally, the scattered intensities found indicated that the crystalline Fe layers were textured. These measurements have not been used for our evaluation, because this would have made a comparison with results from amorphous alloys impossible.) Care was taken to keep the individual layer thicknesses as small as possible to decrease the scattering of electrons from 'bulk-like' (i.e. thick) layers. Both the small individual layer thicknesses and the large numbers of layers making up a 100 nm multilayer film increase the contribution of the interfaces to a measurable extent.

The specimen was coated with a 5 nm Al film both on the top and on the bottom. It was found in previous work [7] that this reliably prevents oxidation of the films and on the other hand does not influence the pdf. Additionally, the substrate was coated with a thin layer of amorphous carbon to allow us to lift the specimen off the substrate after deposition. In this way, a substrate-free specimen could be achieved, without additional scattering by the substrate material.

4. Experiments and results

The experiments were carried out in a conventional TEM (Philips CM30) with an accelerating voltage of 300 kV. The TEM is remotely controllable by an external host computer (PC), which enables the experimenter to retrieve the exact lens settings for one experiment, and after the change of the specimen to restore the microscope settings to

exactly the same electron optical state for another experiment, which is then comparable to the first experiment in the best achievable way. The camera lengths were calibrated before the experiments, and were found to be very precisely reproducible in the different experiments. When the microscope was set up, the diffraction pattern was projected onto a commercial slow-scan CCD camera (Gatan SSC 679), which allowed both a variation of the exposure times over a very wide range, and the registration of the scattered intensity of the camera's signal versus the diffracted intensity with a very high degree of linearity. The linearity was checked for a whole range of exposure times and was in any case found to be perfectly linear within the range used [8].

Typical diffraction patterns exhibit dynamic ranges of $1{:}10^5$ (including the central-beam area), which have to be dealt with. This can be achieved easily with the remote control facility of the TEM, which enables the experimenter to successively shift the diffraction pattern across the faceplate of the camera. In practice, the diffracted intensity was acquired in several successive steps, between which the diffraction pattern was moved across the faceplate of the camera. For each of these successive exposures, the exposure time of the camera was adjusted to make full use of the dynamic range of the camera. By this procedure, it was possible to measure the scattered electron intensities up to high spatial frequencies with an extremely good dynamic range of approximately $1{:}5 \times 10^4$.

After the radial intensity traces were extracted from the recorded image, the data were further processed on a PC with a program which was developed especially for this purpose. The procedure followed was the standard procedure, which has been extensively described elsewhere [9, 10, 11]. It consists in the stripping of the incoherently scattered background contribution from the information-bearing intensity needed. Further processing was done to normalize the scattered intensity according to the atomic form factor of the specimen, averaged according to the atomic composition. This procedure yielded the reduced interference function $i(k)$:

$$i(k) = \frac{I_{\text{exp}}(k) - I_{\text{background}}(k)}{\langle |f(k)|^2 \rangle} \tag{4}$$

with $I_{\text{exp}}(k)$ the experimentally measured scattered electron intensity, $I_{\text{background}}(k)$ the incoherent background contribution, and $\langle |f(k)|^2 \rangle$ the compositionally averaged form factor. The incoherent background is equal to the compositionally averaged form factor, since it represents the scattering of an absolutely random arrangement of atoms of the species contained in the specimen, with definitely no structural information. Therefore, when the inelastic and multiple-scattering contributions can be neglected (which has been shown to be justified in [10, 11]), $I_{\text{background}}(k) = \langle |f(k)|^2 \rangle$, and the above equation becomes

$$i(k) = \frac{I_{\text{exp}}(k) - \langle |f(k)|^2 \rangle}{\langle |f(k)|^2 \rangle} \tag{5}$$

or

$$i(k) = \frac{I_{\text{exp}}(k)}{\langle f(k)^2 \rangle} - 1. \tag{6}$$

This reduced interference function is then subject to a sine transformation in order to obtain the pair distribution function $g(r)$ in real space:

$$4\pi r(\varrho(r) - \varrho_0) = g(r) = \int_{k=0}^{k=\infty} ki(k) \sin(kr)\ \mathrm{d}k. \tag{7}$$

Since the theoretically required upper integration limit $k = \infty$ is not experimentally achievable, the reduced interference function was modulated with a function

$$A(k) = \frac{\sin(\pi k/k_{\max})}{\pi k/k_{\max}} \tag{8}$$

according to Lorch [12] which reduces the termination ripple after the transformation and takes into account the limitation of real-space resolution due to the limited range of spatial frequencies available. This range of spatial frequencies was deliberately limited to a $k_{\max}$ of approximately 120 nm^{-1} for multilayers (figure 5 below), which results in a restricted resolution in real space of only 0.052 nm rather than the usually achievable resolution of 0.017 nm for structurally isotropic amorphous alloys (figure 6 below), when the full range of spatial frequencies accessible is being used for the calculation [9]. The reason for this restriction in the case of the multilayered specimens is the deviation of the Ewald sphere from the x^*–y^*-plane (compare figure 3), which increasingly takes into account intensities that contain information about the z^*-direction in reciprocal space as has been described above. To exclude this unwanted intensity modulation, the cut-off at spatial frequencies of 120 nm^{-1} was necessary for the multilayered specimens.

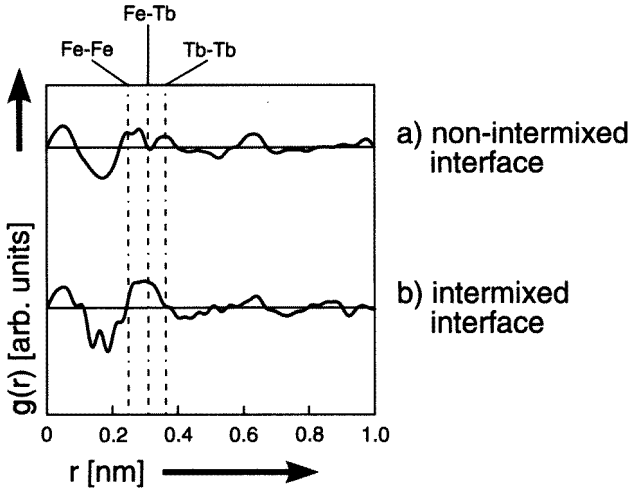

Figure 5. Planar pair distribution functions (p^2dfs) of (a) the sharp-interface specimen and (b) the intermixed-interface specimen. In (a) a decrease in $g(r)$ at an expected Fe–Tb distance can be observed, while in (b)—due to the intermixed interface—the occurrence of Fe–Tb pairs in the plane of the interface can be observed. The known next-neighbour distances for different pairs of atoms are indicated by vertical lines.

The resulting $g(r)$ (equation (7)) will then give maxima whenever the local particle density (considered at a distance r from an arbitrarily chosen atom and averaged over all atoms of the specimen) is larger than the macroscopical mean particle density, averaged over all of the specimen's volume. Therefore, maxima in $g(r)$ give distinct distances of next-neighbour coordination lengths. These next-neighbour coordination lengths are well known for FeTb alloys [13] (both crystalline and amorphous) and give the next-neighbour distances shown in table 1.

It should be noted here that the evaluation according to equation (7) is based on the assumption of a structurally uniform (i.e. non-multilayered) specimen, which is definitely not fulfilled in our experiments on multilayer systems. It is, however, still possible to use

Table 1. Next-neighbour distances in Fe–Tb alloys.

Atomic species	Interatomic distance (nm)
Fe–Fe	0.26
Fe–Tb	0.305
Tb–Tb	0.35

this evaluation of the scattered intensity if the results are used for *comparison* with pdfs of amorphous (i.e. isotropic) alloys of the same composition, only. In this case, *the differences between multilayered and non-multilayered structures* can be seen, which was the aim of this paper. For a quantitative evaluation, a two-dimensional non-isotropic theory [5] has to be used, as it will be in future experiments.

Figures 5(a) and (b) show the resulting pdfs of both the sharp-interface film (figure 5(a)) and the intermixed-interface film (figure 5(b)). Obviously, the intermixed-interface film shows a large maximum of $g(r)$ at the position where a Fe–Tb next-neighbour distance is expected. The pdf shows a broad maximum at around the Fe–Tb next-neighbour distance, which extends also over the indicated positions of Fe–Fe and Tb–Tb next neighbours (a consequence of the deliberately decreased resolution, see above). This corresponds well with the expectations for an intermixed compositionally modulated layer structure.

On the other hand, the sharp-interface film (figure 5(a)) shows two maxima at the positions of Fe–Fe and Tb–Tb next neighbours, but a drop in the pdf to a value of $g(r) \approx 0$ at the position of Fe–Tb next neighbours. This can be interpreted as the pair distribution function of a multilayer structure with only very little intermixing at the interfaces, and therefore no Fe–Tb pairs should be observable in the x–y-plane. This seems, however, not to be exactly the case here, where the number density of Fe–Tb pairs drops only to a value of ϱ_0, which means that the occurrence of Fe–Tb pairs is not zero as one would ideally expect. Instead, a certain degree of intermixing at the interface can still be found—but much less than for the intermixed-interface specimen.

Finally, the effects due to the limited resolution have to be considered in more detail. As mentioned above, the experimental resolution was only 0.052 nm. It is, however, possible to see distinct differences in the p^2dfs in figure 5(a) between the mean separations of Fe–Fe pairs (0.26 nm), Fe–Tb pairs (0.305 nm) and Tb–Tb pairs (0.35 nm). The maxima in the pdfs corresponding to Fe–Tb pairs and Tb–Tb pairs are therefore only 0.045 nm apart. At first sight this seems to be in contradiction to the experimental resolution, but this problem is solved when it is taken into account that the pdfs can assume negative values as well. These negative values mean a below-average density of a specific species of atomic pairs. With respect to the results discussed above, this means that for the sharp-interface film (figure 5(a)) only the pair correlation of the material in the individual layers (i.e. Fe–Fe and Tb–Tb only) can be observed. Due to the sharp interface, the density of Fe–Tb pairs is largely below the value that would be expected for a structurally isotropic (i.e. perfectly intermixed) material, causing a negative value of $g(r)$ at the corresponding position. Together with the positive values of $g(r)$ for both Fe–Fe and Tb–Tb, a decrease in the pair distribution can be observed, even though the separation between individual expected maxima is beyond the resolution limit defined by Rayleigh's criterion.

When an intermixed interface is present (figure 5(b)), the density of Fe–Tb pairs is above average at the separation distance of 0.305 nm, resulting in a positive value of $g(r)$. As a result, due to the limited resolution, no clear separation can be observed between the different species of atomic pairs. The $g(r)$-value for the specific Tb–Tb distance even

drops to approximately zero, which is comparable to the situation for amorphous alloys. This does, however, not necessarily indicate that the short-range order is now amorphous, because the pdf measured is a total pair distribution function, i.e. it takes into account all interatomic next-neighbour separations simultaneously. If, therefore, a partial pdf (for example the Fe–Fe pdf) possesses a minimum at a location where the Tb–Tb distribution would be above average, these two contributions may cancel out.

A comparison of the p^2dfs of multilayer thin films (figure 5) with those of an amorphous alloy of the same nominal composition, as shown in figure 6, leads to the suggestion that the p^2dfs even of the intermixed-interface regions cannot be completely explained in terms of the occurrence of an amorphous, completely intermixed specimen. The p^2dfs differ strongly, which indicates that the multilayer structure is preserved in the samples under investigation here, and also that it is possible to gain new information about the interface quality from planar coordinations.

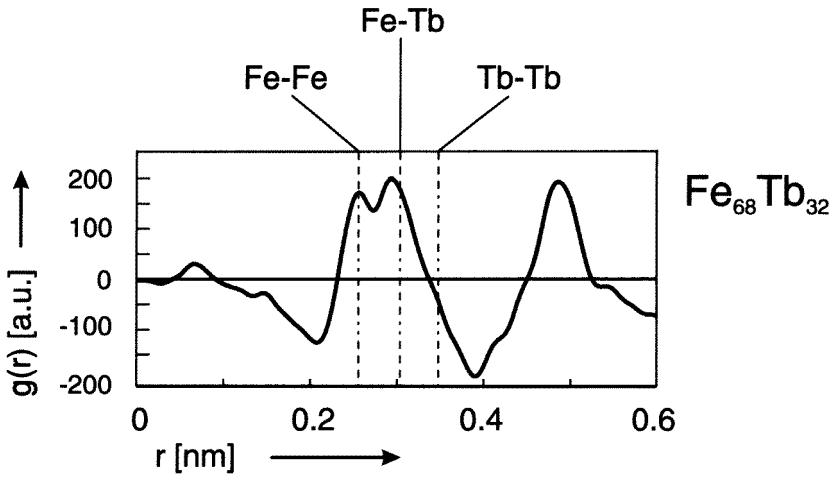

Figure 6. The planar pair distribution function (p^2df) of an amorphous Fe–Tb alloy of a nominal composition comparable to that of the multilayers of figure 5. The different shape proves that a true multilayer structure was investigated, and that the p^2dfs in figure 5 cannot be explained in terms merely of an amorphous alloy due to a complete and homogeneous intermixing of the layers.

It should be noted here that the pdf shown in figure 6 was calculated from data which allowed the usual high resolution to be achieved, since the material was amorphous. Therefore, no truncation of the measured intensity was necessary. In effect, the Fe–Fe and Fe–Tb pairs appear well resolved. At the Tb–Tb interatomic distance a $g(r)$-value of approximately zero can be observed, similarly to the case for figure 5(b). Also, an additional maximum can be seen at approximately 0.48 nm, which is of about the same amplitude as the Fe–Tb maximum. This maximum does not exist with a comparable magnitude in figures 5, indicating that there is a definite structural difference between the amorphous and intermixed multilayer specimens.

5. Summary

A technique has been introduced which takes advantage of the use of high-energy electrons and their large value of $|\boldsymbol{k}|$ for the sensing of pair coordination in a plane parallel to the multilayer thin-film plane. This technique is therefore capable of the measurement of the quality of interfaces of multilayer thin films *inside* a multilayer stack with no further preparation required. The information gained is easily interpretable and straightforward. In particular, no complicated curve-fitting procedures with numerous parameters and the problem of possibly non-unique results is needed.

The application of this technique has been demonstrated on two different types of multilayer thin films of Fe and Tb layers, which have been prepared to have either interfaces that are as sharp as possible or strongly intermixed interfaces. The resulting planar pair distribution functions parallel to the interfaces show the differing related pair distributions. It was also found that the planar pair distribution functions differ significantly from those of amorphous alloys of the same nominal composition, which proves that a *layered* structure could indeed be investigated and distinguished from structurally isotropic amorphous alloys.

References

[1] Sato N and Habu K 1987 *J. Appl. Phys.* **61** 4287
[2] Binasch G, Grünberg P, Saurenbach F and Zinn W 1989 *Phys. Rev.* B **39** 4828
[3] Dorner C, Haidl M and Hoffmann H 1993 *J. Appl. Phys.* **74** 5886
[4] Dorner C, Haidl M and Hoffmann H 1994 *Phys. Status Solidi* a **145** 551
[5] Vainshtein B K 1994 *Fundamentals of Crystals* (Berlin: Springer)
[6] Cowley J M 1981 *Diffraction Physics* (Amsterdam: North-Holland)
[7] Tewes M 1989 *Diploma Thesis* Regensburg
[8] Trautsch R 1995 *Diploma Thesis* Regensburg
[9] Tewes M, Zweck J and Hoffmann H 1994 *J. Phys.: Condens. Matter.* **6** 835
[10] Duscher G 1993 *Diploma Thesis* Regensburg
[11] Zweck J, Duscher G and Tewes M 1994 *Philips Electron Opt. Bull.* **133** 26
[12] Lorch E 1969 *J. Phys. C: Solid State Phys.* **2** 229
[13] Tewes M, Zweck J and Hoffmann H 1991 *J. Magn. Magn. Mater.* **95** 43
[14] Humig S 1994 *PhD Thesis* Regensburg